BIOCOMPATIBILITY AND REGENERATIVE POTENTIAL OF COLLAGEN–KERATIN–HYDROXYAPATITE SCAFFOLDS IN A BILATERAL OSTEOCHONDRAL DEFECT RAT MODEL

Florin POPESCU[1], Florin MICULESCU[2], Irina TITORENCU[3], Madalina ALBU KAYA[4], Niculae TUDOR[5], Adrian BARBILIAN[1]

This study investigates the biocompatibility and regenerative potential of collagen-based scaffolds enriched with keratin and hydroxyapatite in a rat bilateral osteochondral defect model. Three scaffold variants (collagen alone, collagen–hydroxyapatite, and collagen–hydroxyapatite–keratin) were evaluated using FTIR spectroscopy, radiological imaging, and high-resolution micro-CT analysis. The keratin-enriched scaffold showed enhanced bone regeneration, with improved trabecular architecture and mineralization compared to controls. Strong correlations between conventional radiography and micro-CT parameters validated grayscale analysis as a complementary tool for assessing bone regeneration, offering a practical and accessible method to approximate microstructural changes in preclinical studies. These findings highlight the potential of keratin-functionalized biomaterials in osteochondral repair strategies.

Keywords: biomimetic scaffolds, collagen, keratin, hydroxyapatite, bone regeneration, micro-CT, FTIR, immunomodulation, osteochondral repair

1. Introduction

Large bone and osteochondral defects represent a persistent and evolving clinical challenge in human and veterinary medicine. In humans, such lesions are increasingly associated with high-energy trauma, such as traffic accidents and battlefield injuries, often resulting in delayed treatment, long-term disability, and the risk of limb amputation. In veterinary practice, similar defects are encountered

[1] Department of Orthopedics and Traumatology, Faculty of Medicine, University of Medicine and Pharmacy "Carol Davila", Bucharest, Romania, e-mail: popescu_florin_md@yahoo.com
[2] Department of Metallic Materials Science, National University of Science and Technology POLITEHNICA Bucharest, Romania, e-mail: f_miculescu@yahoo.com
[3] Institute of Cellular Biology and Pathology "Nicolae Simionescu", Bucharest, Romania, e-mail: irina.titorencu@gmail.com
[4] National Research and Development Institute for Textiles and Leather, Bucharest, Romania, e-mail: albu_mada@yahoo.com
[5] Faculty of Veterinary Medicine, University of Agronomic Sciences and Veterinary Medicine, Bucharest, Romania, e-mail: niculae.tudor@fmvb.usamv.ro

in high-performance animals and trauma cases, often leading to similar long-term functional impairments.

Conventional treatments, such as autografts and allografts, are often limited by donor site morbidity, immune rejection, and insufficient availability [1, 2]. Consequently, developing biomaterials capable of supporting structural and biological repair in critical-size defects has become an urgent research focus [3–7]. Emerging collagen-bkeratinffolds incorporating bioactive components, such as hydroxyapatite and keratin, offer promising solutions due to their osteoconductive and immunomodulatory properties [1, 8, 9].

2. Materials and methods

Following the design and physicochemical characterization of eight initial experimental scaffold formulations during the biomaterials engineering phase [10], and their subsequent in vitro testing on mesenchymal stem cells (MSCs), three representative variants (F1, F5, and F6) were selected for comprehensive in vivo evaluation. The selected formulations reflect increasing levels of compositional and functional complexity. F1, a pure collagen scaffold [9], served as the control group for evaluating baseline biocompatibility and regenerative potential. F5 combined collagen with hydroxyapatite to assess osteoconductive enhancement, while F6 incorporated both hydroxyapatite and 0.5% (w/v) keratin. The rationale for selecting these three variants was also supported by prior evidence showing that keratin-containing collagen matrices improve structural stability and functional integration in composite biomaterials [11]

2.1 Scaffold preparation

The scaffolds were fabricated following previously validated protocols [10], using type I collagen gel derived from bovine tendon. Hydroxyapatite (HA) was obtained by thermal treatment of bovine bone. Bones were calcined at 1000 °C for 3 hours to eliminate organic components and induce crystallization. The resulting mineral phase was milled and sieved to obtain particles with diameters ranging from 100–200 μm, suitable for osteoconductive integration. HA retains the natural architecture and ionic profile of native bone mineral, enhancing both biocompatibility and resorption dynamics. Keratin (K), sourced from Merck (Darmstadt, Germany), was incorporated at a concentration of 0.5% (w/v). The scaffolds were chemically cross-linked using glutaraldehyde and then frozen to generate porous, three-dimensional structures. Final constructs were sterilized by gamma irradiation prior to implantation.

2.2 In vivo animal model

The current in vivo study was approved by the Ethics Committee of the Cantacuzino National Military-Medical Institute for Research and Development

Bucharest (CI) and authorized by the Sanitary Veterinary and Food Protection Directorate (authorization no. 15/17.05.2023). All experiments were carried out on the CI, Platform of Experimental Medicine, Translational Research and Preclinical Testing Unit, and included 15 adult male Wistar rats. Animals were divided into three groups (n = 5) depending on the material tested. Bilateral femoral defects were created in the intercondylar space of each animal, into which the designated biomaterials were implanted, as previously described [12]. This bilateral model was used to reduce the number of animals while maintaining sufficient experimental power [13, 14].

2.3 FTIR analysis following serum exposure

To complement the initial in vitro characterization and to further validate the in vivo findings, Fourier-Transform Infrared Spectroscopy (FTIR) was used as a supplementary analytical technique. The analysis was conducted at the Faculty of Material Science and Engineering, National University of Science and Technology Polytechnic Bucharest. This aimed to confirm the behavior of the scaffold materials under physiologically relevant conditions, via interaction with biological fluids. Scaffold samples from each group (F1, F5, and F6) were incubated in freshly collected rat serum at 37 °C for 1 hour, 12 hours, and 24 hours, respectively. After each incubation time point, the samples were gently rinsed with phosphate-buffered saline (PBS, pH 7.4). FTIR spectra were then recorded in transmittance mode using an ATR-FTIR spectrophotometer (INTERSPEC 200-X, Interspectrum, Tartumaa, Estonia). This enabled the detection of biochemical interactions occurring at the scaffold surface and the monitoring of time-dependent structural and compositional changes [15]. Specific molecular changes such as protein adsorption, shifts in amide bands, early indications of scaffold degradation, and ionic exchanges were observed. The obtained spectral data were interpreted in comparison to reference profiles of materials in their dry state. The time-resolved evolution of these spectra offered valuable insights into scaffold–serum interactions.

2.4 Radiological and micro-CT imaging

Radiological examinations were performed at the Faculty of Veterinary Medicine, University of Agronomic Sciences and Veterinary Medicine Bucharest, within the Department of Radiology. Digital X-ray imaging was conducted using a certified diagnostic system (DuraDiagnost F30, Philips Healthcare, Suzhou, China). The animals were mildly sedated during imaging procedures to minimize stress and discomfort. For each limb, at least two perpendicular radiographic projections were obtained using standardized positioning protocols. These radiographs were used to evaluate mineralization progression, healing of the intercondylar defect, and cortical alignment. At 12 weeks post-implantation, bilateral femoral samples from two representative animals per group (n = 4 specimens per group) were collected

for high-resolution micro-computed tomography (micro-CT) analysis. Micro-CT scanning was conducted at the Politehnica University of Bucharest using a Bruker SkyScan 2211 nano-CT system (Bruker micro-CT, Kontich, Belgium), which enables high-resolution 3D imaging of trabecular and cortical bone in the intercondylar region. Advanced segmentation techniques for micro-CT image processing were adapted in line with established methodologies for in vivo bone structure analysis [16]. All specimens were scanned under identical parameters: 140 kV source voltage, 200 μA current, no filter, 0.2° rotation step, 7 frames averaging per projection to reduce noise. Image reconstruction was performed using NRecon version 1.7.1.6, with the following settings: 22% beam hardening correction, 13% ring artifact reduction, alignment set to 3, and a smoothing factor of 4. For the analysis of the micro-CT scans, ImageJ (Fiji distribution) was used in combination with the BoneJ2 plugin [14] within the Fiji (ImageJ) software environment. This software combination enabled the extraction of standard three-dimensional morphometric parameters relevant to the assessment of trabecular bone regeneration [17–19].

2.5 Statistical Analysis

Due to the exploratory nature of this preclinical study and ethical constraints on animal use, a formal a priori power analysis was not performed. The study followed the 3Rs principle (Replacement, Reduction, and Refinement) [13], aiming to minimize animal usage while maintaining rigorous data quality through cross-validation of imaging modalities. Unless otherwise noted, data are expressed as mean ± standard deviation (SD), with the number of replicates (n) indicated in each figure legend.Radiographic and micro-CT images were analyzed using ImageJ software (version 1.53t, National Institutes of Health, USA), in combination with the BoneJ2 plugin [14] for three-dimensional morphometric evaluation. For each experimental group, a total of four femoral samples (from two animals, each contributing bilateral femora) were evaluated by micro-CT.Pearson's correlation coefficient (r) was used to assess the relationship between grayscale metrics obtained from radiographs and bone morphometric parameters derived from micro-CT. Statistical analysis was performed using Jamovi (version 2.3.28) and GraphPad Prism 9. The trabecular parameters quantified included bone volume fraction (BV/TV), trabecular thickness (Tb.Th), trabecular spacing (Tb.Sp), and bone surface-to-volume ratio (BS/BV). Given the limited sample size (n = 4), Kruskal–Wallis tests were used descriptively to explore differences across groups.

3. Results and discussions

3.1 ATR-FTIR Analysis

The ATR-FTIR analysis performed on the three scaffold formulations revealed characteristic spectral features indicative of their biochemical composition and interactions with serum components. All samples displayed prominent absorption bands in the regions of 1637–1647 cm^{-1}, 1546–1539 cm^{-1}, and 1237–1239 cm^{-1}, corresponding to the Amide I, Amide II, and Amide III vibrations, respectively. These peaks are associated with C=O stretching, N–H bending, and C–N stretching modes, characteristic of the collagen structure. In the F5 scaffold, an intense band near 1034 cm^{-1} was observed, attributed to the PO_3^- bending and stretching vibrations from hydroxyapatite. This overlapped with a weaker C–O absorption band near 1041 cm^{-1} observed in the collagen-only scaffold (F1).

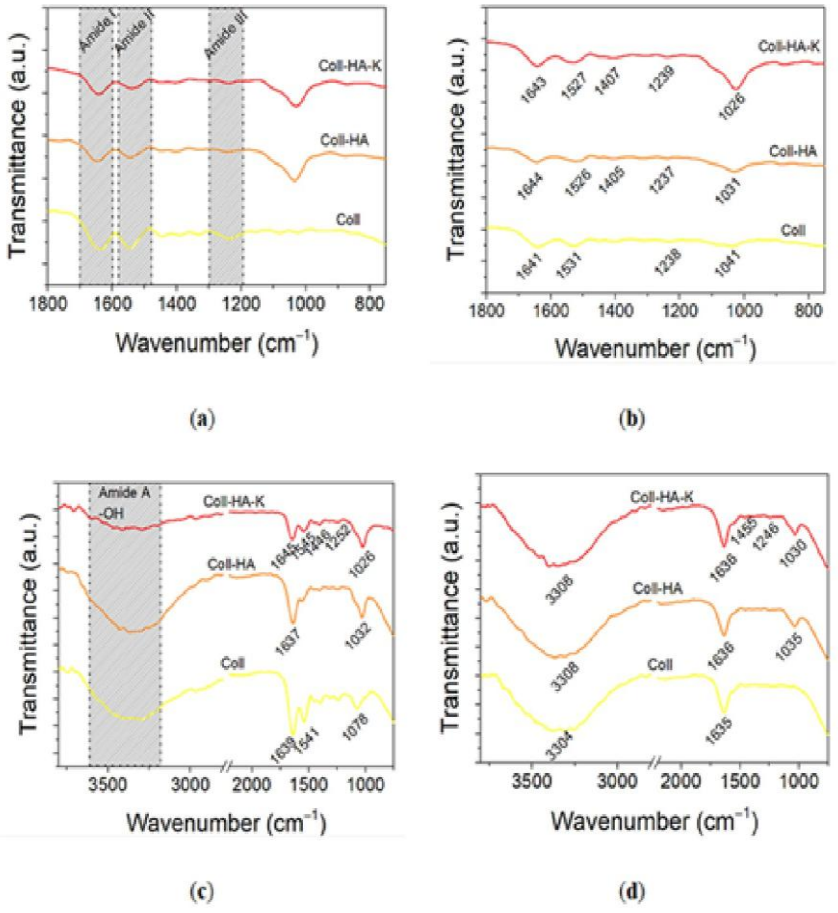

Fig. 1: Comparative ATR-FTIR spectra of collagen-based scaffolds incorporating hydroxyapatite and keratin following exposure to rat serum: (a) Unexposed (initial) scaffold, (b) after 1 hour, (c) after 12 hours, and (d) after 24 hours of serum incubation.

The F6 scaffold presented an additional peak at 1029 cm^{-1}, ascribed to the S–O symmetric stretching of cysteine-S-sulfonate groups, indicating the presence of keratin-specific functional groups. Following 1 hour of serum exposure, a slight reduction in the intensity of the Amide I peak and a minor shift to lower wavenumbers were observed across all scaffold types, consistent with early protein adsorption and hydration. After 12 and 24 hours, a pronounced broad band at approximately 3308 cm^{-1} emerged, corresponding to O–H and N–H stretching vibrations (Amide A), indicative of increasing scaffold hydration and protein interaction.

F5 and F6 scaffolds exhibited overlapping peaks in the 1000–1350 cm^{-1} region, reflecting ongoing ionic exchange between phosphate groups in hydroxyapatite and ions from serum. Notably, the F6 scaffold showed the most intense and shifted Amide I peak after 24 hours, suggesting stronger protein binding capacity and active surface remodeling dynamics.

These findings confirm scaffold–serum interactions that evolve over time, particularly in the F6 group, which showed the greatest shift in Amide I peak intensity and additional spectral changes suggestive of active surface remodeling. This behavior indicates favorable biochemical reactivity and interface adaptability, features that are desirable for osteochondral repair applications requiring rapid protein adsorption and subsequent cellular engagement

3.2 Radiological and micro-CT evaluation

Conventional radiographs obtained at 30 and 60 days revealed progressive mineralization and bone bridging across all experimental groups. The F6 group showed the most uniform grayscale intensity and continuous cortical architecture. Radiological texture analysis using ImageJ [20] demonstrated that F6 had a higher mean grayscale intensity and kurtosis, along with lower standard deviation and skewness values, compared to F1 and F5. These metrics suggest enhanced mineral deposition and improved tissue o indicating a more homogeneous mineral matrix and superior microarchitectural integration. Micro-CT analysis further supported these observations. In the F1 group, large unfilled defects and sparse trabecular structures were noted. The F5 group showed moderate regeneration with partially organized trabeculae and denser architecture. The F6 group exhibited densely packed and well-organized trabeculae with partial defect filling. Quantitative data revealed that F6 achieved a bone volume fraction (BV/TV) of 38.4%, compared to 28.1% in F5 and 16.7% in F1. Trabecular thickness (Tb.Th) in F6 was 0.098 mm, versus 0.074 mm in F5 and 0.052 mm in F1, indicating a more mature and structured trabecular network.

A strong positive correlation was observed between BV/TV and mean grayscale intensity ($r = 1.00$, $p = 0.019$), reinforcing consistency between radiographic and micro-CT assessments. A similar association was found for Tb.Th

(r = 1.00, p = 0.060), though the statistical significance was marginal, likely due to the limited sample size (n = 4). These results further support the utility of grayscale histogram analysis as a semi-quantitative proxy for micro-CT morphometric data.

A central hypodense zone identified in F6 specimens likely reflects residual scaffold undergoing integration. Additionally, triangular radiopaque areas at the superior margin are suggestive of scaffold–bone interface mineralization. Femoral bone segments under 1 cm were scanned using high-resolution micro-CT, with scan durations ranging from 45 to 70 minutes depending on positioning.

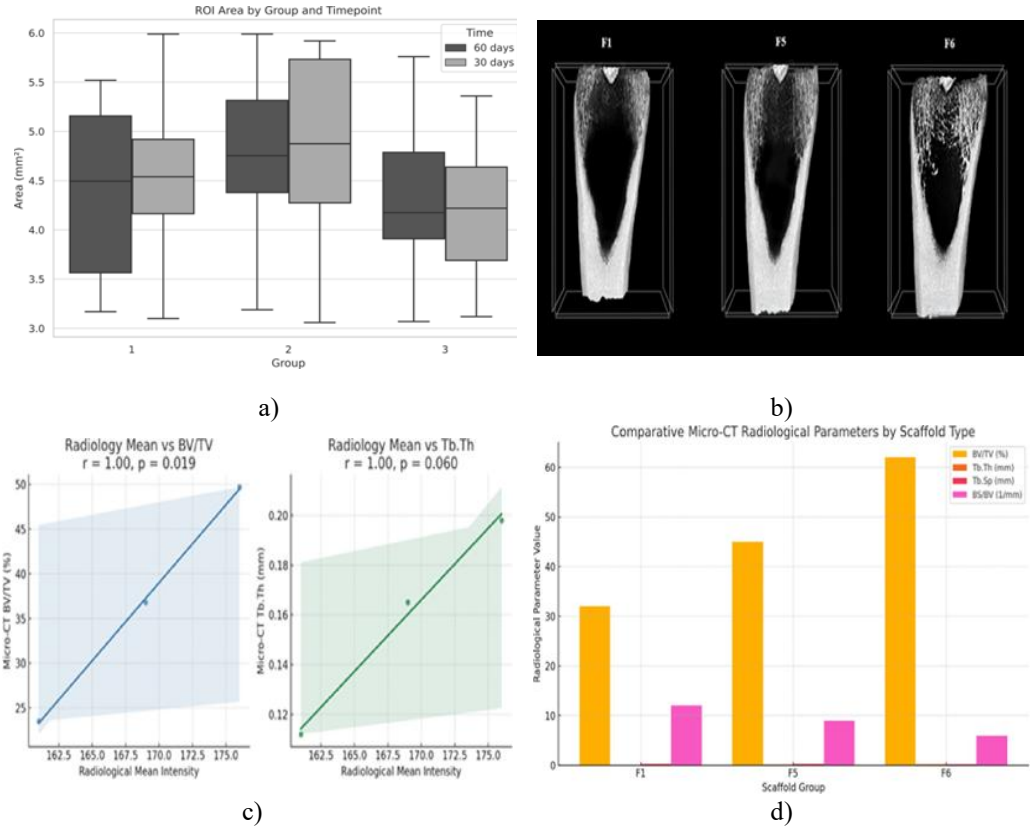

Fig. 2: Comparative view of radiological texture, micro-CT imaging, and morpho-metric analyses: (a) Radiological texture parameters extracted using ImageJ software, illustrating grayscale intensity distribution characteristics relevant to scaffold-mediated bone regeneration. (b) Representative micro-CT image showing the femoral architecture post-implantation. The scan reveals trabecular structure, bone regeneration within the defect area, and scaffold integration. (c) Correlation graphs illustrating the relationship between radiological grayscale intensity and micro-CT derived bone morphometric indices. (d) Radiological parameters assessed using micro-CT across the three scaffold groups (F1, F5, and F6). Morphometric indices such as BV/TV, Tb.Th, Tb.Sp, and BS/BV were extracted and compared to evaluate bone regeneration.

Quantitative evaluation was conducted using the BoneJ plugin within the Fiji (ImageJ) software environment [14], measuring standard morphometric indices: bone volume fraction (BV/TV), trabecular thickness (Tb.Th), trabecular spacing (Tb.Sp), and bone surface-to-volume ratio (BS/BV).

Morphometric data were obtained from bilateral femoral samples harvested from two representative animals per group, yielding a total of four samples per experimental condition (n = 4). Across all parameters, the F6 group showed higher values compared to F1 and F5, supporting the observations from grayscale and micro-CT imaging. These results highlight the value of quantitative imaging techniques in assessing scaffold-mediated bone regeneration in preclinical models.

The application of high-resolution micro-computed tomography to explanted femoral segments enabled three-dimensional analysis of trabecular structure and scaffold integration, complementing in vivo digital radiographic imaging. While conventional X-rays provided an overview of mineralization, micro-CT allowed detailed evaluation of bone microarchitecture and mineral distribution. To assess the predictive value of standard radiographic imaging, grayscale texture parameters extracted from digital X-rays using ImageJ were statistically correlated with morphometric indices obtained via micro-CT at 60 days post-implantation. The aim was to determine whether mean grayscale intensity could reflect key metrics such as BV/TV and Tb.Th.

A strong positive correlation was observed between mean grayscale intensity and BV/TV ($r = 1.00$, $p = 0.019$), with a similar trend for Tb.Th ($r = 1.00$, $p = 0.060$). Although statistical significance for Tb.Th was marginal due to the limited sample size, these results support the use of grayscale texture analysis as a semi-quantitative surrogate for bone quality assessment. The high concordance between radiographic and micro-CT metrics reinforces the potential of integrating accessible imaging methods with digital quantification in scaffold performance evaluation.

4. Discussion

The findings of this study support the hypothesis that composite scaffolds integrating keratin and hydroxyapatite into a collagen matrix offer superior regenerative performance in osteochondral repair compared to simpler biocomposites. The F6 scaffold consistently outperformed the collagen-only (F1) and collagen-hydroxyapatite (F5) variants across all evaluated modalities radiological, microstructural, demonstrating its ability to orchestrate a balanced osteoimmunological environment conducive to regeneration [11]. These results are consistent with hydroxyapatite's osteoconductive capabilities properties [21-24] and keratin's regenerative properties [22].

These results are consistent with hydroxyapatite's osteoconductive capabilities [21–24] and keratin's regenerative and osteoconductive contributions, particularly in keratin–hydroxyapatite composite scaffolds [23, 25, 26]. Keratin may also influence immune signaling pathways and enhance mesenchymal stem cell osteogenic differentiation, reinforcing its relevance in bone tissue engineering [18, 23, 25]. In terms of structural regeneration, the combination of collagen and hydroxyapatite provided a well-established osteoconductive framework, consistent with previous studies [19, 23]. Moreover, keratin has been associated with promoting the osteogenic differentiation of mesenchymal stem cells, further reinforcing its value in bone tissue engineering applications [18].

The correlation between grayscale intensity from digital radiographs and micro-CT-derived metrics (BV/TV and Tb.Th) supports the internal consistency of imaging findings. Image-based texture analysis using ImageJ may represent a useful tool for approximating bone quality in preclinical models, particularly when advanced imaging resources such as micro-CT are limited. These results reinforce the methodological validity of combining radiological and structural assessments in scaffold evaluation [16, 21–27].

Beyond its structural contribution, keratin appears to act as a biologically active component that contributes to both immunomodulation and osteogenic enhancement. Its dynamic role in shaping the local healing environment may be more significant than previously appreciated. However, this study also has limitations. The small sample size, while ethically justified and methodologically optimized, restricts the statistical power and generalizability of the findings. Future studies with expanded cohorts are necessary to confirm these trends and assess long-term integration outcomes.

5. Conclusions

The results of this final in vivo study validate and refine the performance profile of previously developed biomimetic scaffold formulations. Among the tested materials, the F6 scaffold consistently demonstrated systemic safety, regenerative efficacy, and immunological stability in a validated bilateral osteochondral defect model in rats.

In preparation for implantation, the scaffolds were precharacterized using FTIR spectroscopy following exposure to rat serum at 1, 12, and 24 hours. These tests revealed a time-dependent pattern of spectral changes consistent with protein adsorption, surface remodeling, and the early onset of scaffold degradation. These biochemical interactions, particularly in the F6 formulation, support its reactivity and interface adaptability under physiologically relevant conditions.

The imaging techniques used in this study further substantiated the regenerative outcomes. Conventional radiography provided a general overview of

mineralization, while high-resolution micro-computed tomography offered detailed, three-dimensional visualization of trabecular structure and scaffold integration. Quantitative indices, including bone volume fraction and trabecular thickness, confirmed the improved regenerative potential of the keratin–hydroxyapatite–collagen scaffold.

This study also highlights the utility of combining radiological texture analysis with micro-CT evaluation to create a comprehensive framework for scaffold assessment. Future integration with advanced imaging modalities such as MRI or contrast-enhanced CT could further enhance monitoring of scaffold behavior and tissue response in vivo.

Nonetheless, the study was limited to a single terminal timepoint (12 weeks), which restricts conclusions regarding scaffold degradation kinetics and long-term remodeling. Future longitudinal studies are needed to address these aspects and support progression toward large-animal studies and clinical translation.

REFERENCES

[1] P. Baldwin, D.J. Li, D.A. Auston, H.S. Mir, R.S. Yoon, and K.J. Koval. Auto- graft, allograft, and bone graft substitutes: Clinical evidence and indications for use in the setting of orthopaedic trauma surgery. Journal of Orthopaedic Trauma, 33(4):203–213, 2019.

[2] K.M. Salleh and N.F. Abd Rashid. Keratin-based biomaterials for biomedical applications. In Polymer Composites Derived from Animal Sources, pages 219–242. Elsevier, 2024.

[3] S.V. Dorozhkin. Calcium orthophosphate-based bioceramics. Materials, 6(9):3840–3942, 2013.

[4] H. Hwangbo, H. Lee, E.J. Roh, W. Kim, H.P. Joshi, and S.Y. Kwon. Bone tissue engineering via application of a collagen/hydroxyapatite 4d-printed biomimetic scaffold for spinal fusion. Applied Physics Reviews, 8(2):021403, 2021.

[5] P. Nitti, S.K. Padmanabhan, S. Cortazzi, E. Stanca, L. Siculella, A. Licciulli, and C. Demitri. Enhancing bioactivity of hydroxyapatite scaffolds using fibrous type i collagen. Frontiers in Bioengineering and Biotechnology, 9:631177, 2021.

[6] A. Maidaniuc, M. Miculescu, S.I. Voicu, L.T. Ciocan, M. Niculescu, M.C. Corobea, M.E. Rada, F. Miculescu, Effect of micron sized silver particles concentration on the adhesion induced by sintering and antibacterial properties of hydroxyapatite microcomposites, Journal of Adhesion Science and Technology, 30(17):1829-1841, 2016.

[7] M. Mindroiu, E. Cicek, F. Miculescu, I. Demetrescu, The influence of thermal oxidation treatment on the electrochemical stability of TiAlV and TiAlFe alloys and their potential application as biomaterials, Revista de Chimie, 58(9):898-903, 2007.

[8] S. Vermeulen, M. Van Dyck, and E.J.M. Van Damme. Keratin-based biomaterials: a review of protein chemistry and applications in regenerative medicine. Materials Science and Engineering C, 118:111478, 2021.

[9] A. Vasconcelos and A. Cavaco-Paulo. The use of keratin in biomedical applications. Current Drug Targets, 14(5):612–619, 2013.

[10] F. Popescu, I. Titorencu, M. Albu Kaya, F. Miculescu, R. Tutuianu, A.E. Coman, et al. Development of innovative biocomposites with collagen, keratin and hydroxyapatite for bone tissue engineering. Biomimetics, 9(7):428, 2024.

[11] X. Wu, Y. Luo, Q. Liu, S. Jiang, and G. Mu. Improved structure-stability and packaging characters of crosslinked collagen fiber-based film with casein, keratin and spi. Journal of the Science of Food and Agriculture, 99(11):4942–4951, 2019.

[12] D.L. Ancuta, M. Crivineanu, T. Soare, and C. Coman. In vivo effects of titanium implants treated with biomaterials in the bone regeneration process. Scientific Works Series C Veterinary Medicine, 66:155–160, 2021.

[13] K.H. Lee, D.W. Lee, and B.C. Kang. The ‘r’ principles in laboratory animal experiments. Laboratory Animal Research, 36(1):45, 2020.

[14] M. Ito. Animal models for bone and joint disease. assessment of bone mass, struc- ture and strength in rat and mouse models - focus on micro-computed tomography study. Clinical Calcium, 21(2):242–252, 2011.

[15] M. Raˆpaˇ, C. Gaidaˇu, L.M. Stefan, E. Matei, M. Niculescu, M.D. Berechet, et al. New nanofibers based on protein by-products with bioactive potential for tissue engineering. Materials, 13(14):3149, 2020.

[16] J.H. Waarsing, J.S. Day, and H. Weinans. An improved segmentation method for in vivo microct imaging. Journal of Bone and Mineral Research, 19(10):1640–1650, 2004.

[17] M. Doube, M.M. Kłosowski, I. Arganda-Carreras, F.P. Cordelie`res, R.P. Dougherty, J.S. Jackson, et al. Bonej: Free and extensible bone image analysis in imagej. Bone, 47(6):1076–1079, 2010.

[18] J. Schindelin, I. Arganda-Carreras, E. Frise, V. Kaynig, M. Longair, T. Pietzsch, et al. Fiji: an open-source platform for biological-image analysis. Nature Methods, 9(7):676–682, 2012.

[19] E. Kokkinou, I. Boniatis, L. Costaridou, A. Saridis, E. Panagiotopoulos, and G. Panayiotakis. Monitoring of bone regeneration process by means of texture analysis. Journal of Instrumentation, 4(09):P09007, 2009.

[20] F. Popescu, M.G. Albu Kaya, F. Miculescu, A.E. Coman, D.L. Ancuta, C. Coman, and A. Barbilian. Novel collagenous sponge composites for osteochondral regeneration in rat knee models: A comparative study of keratin, hydroxyapatite, and combined treatments. Cureus, 16(11):e73428, 2024.

[21] L. Mendes, G. Ribeiro, and R. Marques. In situ hydroxyapatite synthesis: Influence of collagen on its structural and morphological characteristic. Materials Sciences and Applications, 3:580–586, 2012.

[22] F. Miculescu, A. Maidaniuc, M. Miculescu, N.D. Batalu, R.C. Ciocoiu, S.I Voicu, G.E. Stan, V.K. Thakur, Synthesis and Characterization of Jellified Composites from Bovine Bone-Derived Hydroxyapatite and Starch as Precursors for Robocasting, ACS OMEGA, 3(1):1338-1349, 2018.

[23] F. Miculescu, A.C. Mocanu, G.E. Stan, M. Miculescu, A. Maidaniuc, A. Cîmpean, V. Mitran, S.I. Voicu, T. Machedon-Pisu, L.T. Ciocan, Influence of the modulated two-step synthesis of biogenic hydroxyapatite on biomimetic products' surface, Applied Surface Science, 438: 147-157, 2018.

[24] V. Mitran, R. Ion, F. Miculescu, M.G. Necula, A.C. Mocanu, G.E. Stan, I.V. Antoniac, A. Cimpean, Osteoblast Cell Response to Naturally Derived Calcium Phosphate-Based Materials, Materials, 11(7), Art. No. 1097, 2018.

[25] G.J. Dias, P. Mahoney, N.A. Hung, L.A. Sharma, P. Kalita, R.A. Smith, et al. Osteoconduction in keratin-hydroxyapatite composite bone-graft substitutes. Journal of Biomedical Materials Research Part B: Applied Biomaterials, 105(7):2034– 2044, 2017.

[26] M.L. Bouxsein, S.K. Boyd, B.A. Christiansen, R.E. Guldberg, K.J. Jepsen, and R. Muller. Guidelines for assessment of bone microstructure in rodents using micro-computed tomography. Journal of Bone and Mineral Research, 25(7):1468– 1486, 2010.

[27] R.Z. LeGeros. Calcium phosphate-based osteoinductive materials. Chemical Reviews, 108(11):4742–4753, 2008.